

IAC-10-D9.2.8

STRUCTURAL ANALYSIS AND PRELIMINARY SPACE CHARACTERIZATION OF A PROTOTYPE
HOLLOW LASER RETROREFLECTOR.

C. Cantone

Laboratori Nazionali di Frascati (LNF) dell'INFN, Frascati (Rome), claudio.cantone@lnf.infn.it

R. Napolitano

Laboratori Nazionali di Frascati (LNF) dell'INFN, Frascati (Rome), rnapolitano@email.it

M. Tibuzzi

Laboratori Nazionali di Frascati (LNF) dell'INFN, Frascati (Rome), mattia.tibuzzi@lnf.infn.it

S. Dell' Agnello

Laboratori Nazionali di Frascati (LNF) dell'INFN, Frascati (Rome), simone.dellagnello@lnf.infn.it

G. O. Delle Monache

Laboratori Nazionali di Frascati (LNF) dell'INFN, Frascati (Rome), giovanni.dellemonache@lnf.infn.it

R. Tauraso

University of Rome Tor Vergata and INFN-LNF, Rome, Italy, roberto.tauraso@uniroma2.it

F. Vivio

University of Rome Tor Vergata, Rome, Italy, vivio@uniroma2.it

M. Garattini

Laboratori Nazionali di Frascati (LNF) dell'INFN, Frascati (Rome), marco.garattini@lnf.infn.it

A. Boni

Laboratori Nazionali di Frascati (LNF) dell'INFN, Frascati (Rome), alessandro.boni@lnf.infn.it

C. Lops

Laboratori Nazionali di Frascati (LNF) dell'INFN, Frascati (Rome), caterina.lops@lnf.infn.it

S. Berardi

Laboratori Nazionali di Frascati (LNF) dell'INFN, Frascati (Rome), simone.berardi@lnf.infn.it

R. Vittori

Aeronautica Militare Italiana (AMI) and Agenzia Spaziale Italiana (ASI), Rome, Roberto.Vittori@pg.infn.it

C. Powell

Goddard Space Flight Center, Cory.A.Powell@nasa.gov

J. McGarry

Goddard Space Flight Center, Jan.McGarry@nasa.gov

D. A. Arnold

Harvard-Smithsonian Center for Astrophysics (CfA), Cambridge, MA, USA, david-arnold2006@earthlink.net

M. R. Pearlman

Harvard-Smithsonian Center for Astrophysics (CfA), Cambridge, MA, USA, mpearlman@cfa.harvard.edu

M. Maiello

Laboratori Nazionali di Frascati (LNF) dell'INFN, Frascati (Rome), mauro.maiello@lnf.infn.it

L. Porcelli

Laboratori Nazionali di Frascati (LNF) dell'INFN, Frascati (Rome), luca.porcelli@lnf.infn.it

N. Intaglietta

Laboratori Nazionali di Frascati (LNF) dell'INFN, Frascati (Rome), nicola.intaglietta@lnf.infn.it

M. Martini

Laboratori Nazionali di Frascati (LNF) dell'INFN, Frascati (Rome), manuele.martini@lnf.infn.it

A new kind of Cube Corner Retroreflector (CCR) for Satellite Laser Ranging (SLR) has been modeled from the structural point of view. Traditional CCRs are solid pieces of fused silica while this new kind of CCR is hollow. This means that there are only the three reflecting surfaces without the bulk volume material whose index of refraction and, therefore, optical performance is affected by thermal gradients which may develop in space conditions. In addition, hollow cubes allow a significant lightening of all laser ranged payloads. However, it is difficult to manufacture hollow CCRs which maintain structural integrity and optical performance in the harsh space environment. We are mainly interested in the application of hollow CCRs to future Global Navigation Satellite System (GNSS) constellations. since, coupling traditional microwave ranging of GNSS constellation with laser ranging, will improve the accuracy on the positioning, and then the performance of the system, but will also provide important data for gravitational Physics. The optical behavior of a retroreflector is given by its Far Field Diffraction Pattern (FFDP). Inside the Frascati National Laboratories (LNF) of the Italian National Institute for Research in Nuclear Physics (INFN), near Rome, there is an experimental apparatus, the SCF, designed to measure the FFDP of CCRs kept in a representative space environment. INFN, together with the Italian Space Agency (ASI) is starting a project to develop, build and test an optimized GNSS retroreflector array, including also the characterization of hollow retroreflectors in collaboration with NASA-GSFC. In fact, hollow cubes are structurally weaker than solid ones and they need refined analyses to understand the relationship between thermal deformation and optical performance. Several simulations have been developed using the finite element commercial software ANSYS[®]. The interaction between the faces through the connecting glue has been the core of the finite element study. A versatile post-processing technique has been used to compute, from the results of the simulation, the peak to valley distance over each deformed face and the mutual position among them i.e. the alteration of dihedral angles; both these parameters give information on the optical performance of the retroreflector before measuring its FFDP. The comparison between simulation and experimental data is also shown in this paper.

I. HOLLOW CUBES INSIDE THE ETRUSCO 2 PROJECT

Since the Apollo 11 mission in 1969, Cube Corner Retroreflectors (CCRs) have provided precious data for research in fundamental physics and geodesy. They are completely passive devices which show almost no aging.

CCRs equipped space satellites and payloads, are monitored by the International Laser Ranging Service (ILRS) which aims to support geodetic and geophysical research activities (1). These CCRs, even though made of different materials, are all solid pieces: laser photons go through the body, bounce thrice, once over each reflecting surface of the cube corner, and come back the same direction they came from. Time flight measurement give very precise information on the CCR position.

Thermal gradients, changing the light refraction index along the photon path, negatively affect the optical performance. Photons back to the Earth, spread over a spatial energy distribution, the Far Field Diffraction Pattern (FFDP) which is carefully designed to take account of the relative movement between the

satellite and the ground stations; as we said before, thermal gradients affect the FFDP.

A new experimental apparatus, the Satellite-lunar laser ranging Characterization Facility (SCF), has been set inside the Frascati National Laboratories (LNF) of INFN, which is the Italian National Institute for research in Nuclear Physics (2). SCF-Test would address two basic issues: (i) the design of an optimized laser reflector payload for Galileo, that is the next coming European Global Navigation Satellite System (GNSS), (ii) the pre-launch evaluation of the 'as-built' functionality of laser retroreflector payloads in representative space conditions. ILRS has still expressed its standards about laser ranged payloads optical performance in order to have GNSS satellites suitably monitored (3). The SCF-Test was developed in 2006-09, in the context of ETRUSCO, an interdisciplinary INFN experiment at LNF and it is background intellectual property of INFN; we proposed it as such for the simulation and testing of the SLR of Galileo, as well as of other GNSS constellations, and of the 2nd generation LLR (Lunar Laser Ranging) for new lunar missions (4), (5), (6) and (7).

A project of technological development, whose name is ETRUSCO-2, has been co-funded by ASI and INFN over the period 2010-2012. A comprehensive and non-invasive space characterization like the SCF-Test has never been performed before: thanks to its superior Hydrogen-maser atomic clocks and the proposed SCF-Test of retroreflectors, Galileo can provide a large improvement in the measurement of its gravitational redshift.

The project include also, in collaboration with NASA Goddard Space Flight Center (GSFC), the simulation and testing of hollow reflectors; hollow means that there is no bulk material but only the three reflecting surfaces, joined together through some adhesive (8), (9). Hollow cubes are significantly lighter than traditional ones. Even though thermal gradients have no longer effect on the refraction index, since there is no bulk material, the thermal behaviour of the CCR still influences the FFDP, because thermal deformations can reduce the flatness of each mirror and can also change their mutual positions: the structural design, that is almost useless for solid reflectors, becomes here the real focus.

II. PRE-TESTING ANALISYS

Before setting up the experimental test, we carried on some simulations considering three possible designs of hollow cubes which differ each other both for the material and for the shape:




	Beryllium Hollow Cube Corner Retroreflector $E = 289 \text{ GPa}$ $\nu = 0.1$ $\rho = 1854 \text{ Kg/m}^3$ $\alpha = 11.2 \text{ E-6 K}^{-1}$
	Extreme Temperature Retroreflector (ETR) $E = 68.94 \text{ GPa}$ $\nu = 0.33$ $\rho = 2712 \text{ Kg/m}^3$ $\alpha = 2.34 \text{ E-5 K}^{-1}$
	Zerodur/Pyrex Hollow Cube Corner Retroreflector $E_z = 91 \text{ GPa}$ $\nu_z = 0.243$ $\rho_z = 2530 \text{ Kg/m}^3$ $\alpha_z = 0.05 \text{ E-6 K}^{-1}$ $E_p = 62.75 \text{ GPa}$ $\nu_p = 0.2$ $\rho_p = 2230 \text{ Kg/m}^3$ $\alpha_p = 3.25 \text{ E-6 K}^{-1}$

Table I: Three different designs for hollow CCRs

The third shape comes in two different materials: Zerodur and Pyrex but, in the following, we will refer to it as Zerodur design.

Glue strips finite element modelling

The most difficult aspect has been modelling suitably the glue strips which join together the mirrors: since they are very slim, you cannot size your brick elements according to them, otherwise it would result in a huge number of nodes for all the rest of the model, even designing a transition mesh among the glued edges and the remaining part of the mirror.

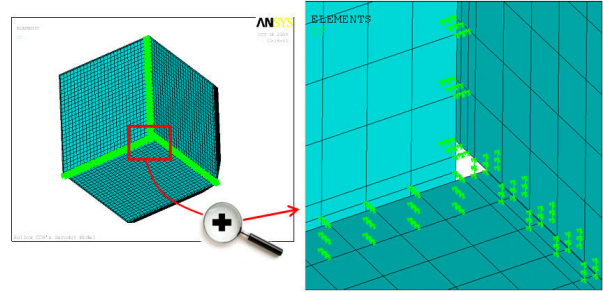


Fig. I: Finite element graphical representation of the spring based glue connection.

In order to address this issue, we tried two complementary approaches: the first one uses three orthogonal springs, one for traction and two for shear, per every couple of facing nodes; only mapped meshes, precisely designed to have straight corresponding nodes on the mirrors, like we did, can be used for automatic implementation of this method.

The second approach uses the sub-structuring technique: the glue strips are modelled with a very fine mesh; then the stiffness matrix of this finite element model, which is called super element, is Guyan condensed to just some degrees of freedom (DOFs) which are those used for interface with the stiffness matrix of the mirrors. The finer mesh of the glue strip has a division pattern that is multiple of the coarser mesh of the mirrors; this way, all the mirror nodes placed on the glued edge have the same coordinates of some other nodes belonging to the strip model. The script which automatically generates the finite element models, in order to size the mapped meshes, needs just two parameters: the division number along the mirror edge and the multiplication factor for the glue strip division. The stiffness matrix of the glue strip is Guyan condensed to the DOFs of these nodes which are called master nodes of the super element while all the remaining ones are called slave nodes. This is, in general, a key aspect of sub-structuring: you want to

condense a group of regular* finite elements into a single superelement which will be after included in the main model; condensation is done by identifying a set of master degrees of freedom and considering the stiffness matrix of the complete sub-structure, define the relationships between themselves. From the point of view of the main model the superelement becomes this way a black box, you do not really know what happens inside it but you know that the master degrees of freedom correctly account all the sub-structure. When we say “correctly”, we do not say completely the truth: the condensation of the stiffness matrix is always exact but, during condensation, you also transfer the mass of slave nodes on the master ones; the last operation is always an approximation since you are actually moving some mass from one place to another one. For this reason, you could have likely heard that Guyan condensation is correct only in static analysis while it is approximated in dynamics and in every other application where the mass distribution plays its role.

As far as concerns applying loads, you can do that either after including the sub-structure inside the main model or in advance. If you have any dynamic effect you should apply loads in advance in order to correctly account the mass distribution. If the analysis is a static one, it makes no difference when you apply loads.

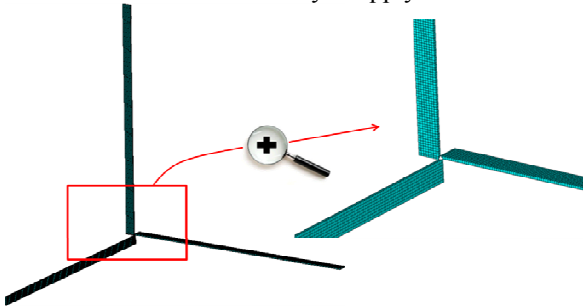


Fig. II: Finite element model of the glue strips

When you place one or more super elements inside a main model with other non super elements, the stiffness matrix of this analysis refers to all the degrees of freedom of non super elements, but only to the master degrees of freedom of the superelement i.e. there is no trace in this stiffness matrix of the slave DOFs of the sub-structure, but their contribute to the main model deformation is truly accounted by the masters. When we say stiffness matrix, of course, we are thinking to a structural analysis but you can use sub-structuring for every kind of analysis.

Thermal distortion simulations

* With regular we mean every kind of basic element offered by the software, in contrast with super element which is designed, both the shape and the structural behavior, by the user.

In the case of hollow CCRs, the thermal distortions are directly connected with the optical behaviour.

The first step was to recognize which kind of simulation tests would be more interesting to shortly characterize the CCRs; we did not have at that moment any experimental data and we chose to load the reflectors with two different kinds of applied temperature field: a thermal gradient along the symmetry axis and a bulk temperature homogeneous increase. We also combined the studies adding a gradient over a bulk increase.

Every object sent in space, experiences two different electro magnetic radiation fields. It may be considered inside an all surrounding cold environment at 2.73 Kelvin but loaded by an hot source, the Sun, which outside the atmosphere supplies 1367 W/m^2 ; this value is defined by the AM0 standard, where the acronym stands for Air Mass zero i.e. without atmosphere; the same standard compare the actual Sun spectrum with an ideal black body radiation at the temperature of 5777 K ; this is considered to be the apparent superficial temperature of the Sun. The mean temperature of the object is, for this reason, given by the ratio between the solar absorptivity and the infra red emissivity of its external surface. Under these two strong opposite loads, the mean temperature of many different objects is usually around 300 K : this is actually the guess value for the reference temperature we gave to all our models. Reference temperature is that one where you do not have any thermal stress.

According with this hypothesis, the three different applied thermal fields were:

- one Kelvin degree gradient along the symmetry axis from 301 K to 300 K
- 380 bulk, homogeneous, temperature
- the combination of the previous two fields: a gradient from 381 K to 380 K

The tip of the CCR, that is also the origin of the coordinate system, is warmer than all the other points and the temperature decreases linearly while you move along the CCR symmetry axis which is in our model also the “z” axis of the main frame of reference. This choice would be helpful for anyone intentioned to develop other models.

In the first thermal field we assign to the origin node a temperature of 301 K we linearly reach 300 K for the nodes with the maximum value of z coordinate, which in the cases of Zerodur and Beryllium design, they are just three nodes, while for the ETR design, they are all the nodes belonging to the chamfer (look at Fig. III).

Optical integrity analysis

After the solution of the thermal distortion analysis, we extract from ANSYS® the starting positions and the displacements for all the nodes belonging to the mirrors. These data will be post-processed through MATLAB® in order to find out if the thermal distortion would warp

the mirrors beyond the limit that can be considered acceptable.

There are two different checks to perform:

- Peak to Valley (P-V) flatness.
- Cube Dihedral Angle deformations (Δ CDA).

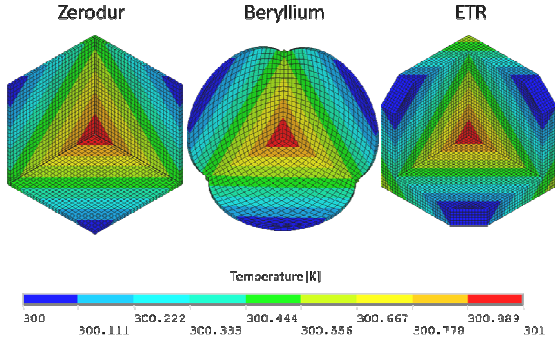


Fig. III: One Kelvin linear gradient load field on all the three simulated designs

The first one refers to the difference, in terms of normal distance from the mirror surface, between the highest and lowest point: it must not exceed $0.025 \mu\text{m}$ that is about the twentieth part of the green laser wavelength, $0.532 \mu\text{m}$.

As far as concerns cube dihedral angles, they must be kept within $\Delta\text{CDA} = \pm 0.5''$ of tolerance. We compute the variation of the cube dihedral angle this way: $(\Delta\text{CDA}) = \alpha_{\text{warp}} - 90^\circ$, where α_{warp} is the angle between the warped mirrors; in the case of no warping $\alpha_{\text{warp}} = 90^\circ$.

In order to evaluate the aforementioned optical criteria, we started deriving, for every mirror in not deformed configuration, its mathematical expression in the form $ax + by + cz + d = 0$, where a, b and c are the coordinates of the plane normal vector:

Plane 1	$-0.8165x + 4.0708e-016y + 0.5774z + 0 = 0$
Plane 2	$0.4082x - 0.7071y + 0.5774z - 1.2690e-04 = 0$
Plane 3	$0.4082x + 0.7071y + 0.5774z + 7.3056e-20 = 0$

Table II: equations for not deformed mirrors; the way we built the model makes these equations the same for all the three different designs

You can get them easily just choosing three points (the origin, O, and 2 corners, namely P_2 and P_3 , per every mirror) and then, the normal vector direction, is given by the cross-product between these two vectors ($\overline{OP_3}$ and $\overline{OP_2}$). We finally normalize these vectors and makes them pointing inward the CCR setting the third component to be positive.

Both checking P-V and Δ CDA, need a surface fit of the cloud of points, which all moved as a consequence of thermal load, from the starting mirror plane. We tried to fit this points distribution with another plane, which obviously comes to be different from the not deformed one. This is the easiest choice; in the future we will try to fit the cloud with a second order surface with a smoother shape and a saddle point in the origin of the coordinate system.

The only assumption for the planar fitting is that the z-component of the data is functionally dependent on the x- and y-components i.e. you would never apply the following formulas in the case of fitting planes orthogonal to the x-y plane.

Basically: given a set of points $\{(x_i, y_i, z_i)\}_{i=1}^m$, you determine A, B, and C so that the plane $z = Ax + By + C$ best fits the samples: we want that, the sum of the squared errors between the z_i , that are the samples third components, and the values $Ax_i + By_i + C$, that are, in turn, the third components of points belonging to the fitting plane, is minimized. Note that the error is measured along the z-direction and not in the direction orthogonal to the plane. Then, if you define this way the error function:

$$E(A,B,C) = \sum_{i=1}^m [(Ax_i + By_i + C) - z_i]^2 \quad [1]$$

you can easily see that this function is nonnegative and its graph is a Hyper-paraboloid whose only minimum occurs when the gradient satisfies $\nabla E = (0,0,0)$. This leads to a system of three linear equations in A, B, and C which can be easily solved. Precisely:

$$(0,0,0) = \nabla E = 2 \sum_{i=1}^m [(Ax_i + By_i + C) - z_i] (x_i, y_i, 1) \quad [2]$$

And then, the same of [2] but in matrix form:

$$\begin{bmatrix} \sum_{i=1}^m x_i^2 & \sum_{i=1}^m x_i y_i & \sum_{i=1}^m x_i \\ \sum_{i=1}^m x_i y_i & \sum_{i=1}^m y_i^2 & \sum_{i=1}^m y_i \\ \sum_{i=1}^m x_i & \sum_{i=1}^m y_i & \sum_{i=1}^m 1 \end{bmatrix} \begin{bmatrix} A \\ B \\ C \end{bmatrix} = \begin{bmatrix} \sum_{i=1}^m x_i z_i \\ \sum_{i=1}^m y_i z_i \\ \sum_{i=1}^m z_i \end{bmatrix} \quad [3]$$

The solution provides the least squares solution $z = Ax + By + C$. At this point, you can easily change this equation of the plane in the form $ax+by+cz+d = 0$. Of course it stands:

$$z = (-a/c)x + (-b/c)y + (-d/c)$$

and then, solving the following system,

$$\begin{cases} A = -\frac{a}{c} \\ B = -\frac{b}{c} \\ C = -\frac{d}{c} \end{cases} \Rightarrow A^2c^2 + B^2c^2 + c^2 = 1 \rightarrow c = \pm \sqrt{\frac{1}{A^2 + B^2 + 1}}$$

$$a^2 + b^2 + c^2 = 1$$

you reach the desired expression; we choose the “+” sign in order to obtain the normal vector pointing inward the CCR.

Now that we have the fitting planes and their normal vectors, we can compute for every node “i” the distance d_i from its fitting plane that is of course given by the dot product with the plane normal vector:

$$d_i = \begin{pmatrix} n_x & n_y & n_z \end{pmatrix} \begin{pmatrix} x_i \\ y_i \\ z_i \end{pmatrix}$$

and organize all these distances, for every mirror, in a vector \vec{d} . The peak to valley flatness is the difference between the maximum and the minimum distances:

$$P-V = \max(\vec{d}) - \min(\vec{d}) \quad [4]$$

	P-V _{max} = 0.025μm ≈ 0.047*λ _{green}		Δ CDA _{max} = ± 0.5"	
	Peak to Valley (P-V) / λ _{green}		ΔCube Dihedral Angle ["]	
ΔT = 300 ÷ 301 K	Plane 1	0.0387	Planes 1-2	0.3073
	Plane 2	0.0357	Planes 1-3	0.3053
	Plane 3	0.0402	Planes 2-3	0.2962
T _{Bulk} = 380 K	Plane 1	4.2	Planes 1-2	10.8693
	Plane 2	3.7417	Planes 1-3	8.889
	Plane 3	4.1596	Planes 2-3	11.4006
ΔT = 380 ÷ 381 K	Plane 1	4.2242	Planes 1-2	11.1766
	Plane 2	3.7668	Planes 1-3	9.1942
	Plane 3	4.1864	Planes 2-3	11.6967

Table III: Optical integrity simulations summary table for the Zerodur design

	P-V _{max} = 0.025μm ≈ 0.047*λ _{green}		Δ CDA _{max} = ± 0.5"	
	Peak to Valley (P-V) / λ _{green}		ΔCube Dihedral Angle ["]	
ΔT = 300 ÷ 301 K	Plane 1	0,0830	Planes 1-2	0,7167
	Plane 2	0,0346	Planes 1-3	0,6934
	Plane 3	0,0315	Planes 2-3	0,5796
T _{Bulk} = 380 K	Plane 1	8,3601	Planes 1-2	19,5448
	Plane 2	4,6963	Planes 1-3	15,5104
	Plane 3	4,2956	Planes 2-3	18,3094
ΔT = 380 ÷ 381 K	Plane 1	8,4236	Planes 1-2	20,2612
	Plane 2	4,7159	Planes 1-3	16,2036
	Plane 3	4,3034	Planes 2-3	18,8890

Table IV: Optical integrity simulations summary table for the Pyrex CCR

While the angle between the fitted planes, let us consider only planes number 1 and 2, is given by the inverse cosine of the dot product between the normal vectors, like in equation number [5]:

$$\alpha_{warp,1-2} = a \cos(\vec{n}_1 \cdot \vec{n}_2) \quad [5]$$

The summary about the three applied temperature fields is given, for the Zerodur design, that is at the moment the best candidate to fly, in Table III. The Goddard researchers recognized in the glue coefficient of thermal expansion (CTE), the main reason of malfunctioning under thermal loads. It is underlined in their study that the CTE of glue (87 e-6 K⁻¹) is too much compared with the same parameter for Zerodur (0.05 e-6 K⁻¹). This mismatch causes high tensions at the interface which, in turn, deform the mirrors. They asked for this reason to the manufacturer, to make the same object in Pyrex, instead of in Zerodur. Pyrex has a CTE of 3.25 e-6 K⁻¹ which is much closer to the glue CTE but, unfortunately, it has a Young’s module lower than the other: it is 62.75 GPa instead of 91 GPa. We show in Table IV the summary for the optical integrity, concerning the cube corner in Pyrex. The comparison with Table III clearly shows that things got worse. Moreover, the mismatch is certainly a problem but, if your mirror has a higher CTE, it is more deformed by the thermal load: even if you have reduced the mechanical action of the glue, you have increased the effect of the thermal load.

III. EXPERIMENTAL ACTIVITY

The experimental apparatus we use, is set inside LNF and it is named SCF (Satellite-lunar laser ranging Characterization Facility). An external view of the SCF and of the optical table equipped beside the cryostat, is shown in Fig. IV.

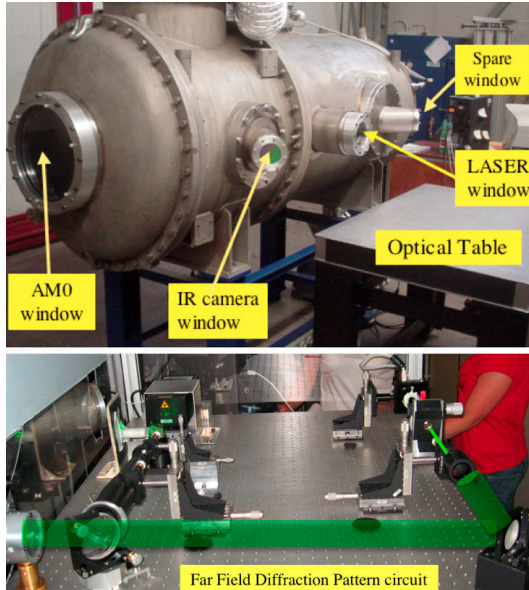


Fig. IV: External cryostat with its window and optical table equipped for FFDP measurements.

The steel cryostat has a length of about 2 m and a diameter of about 0.9 m. On one side the cryostat has three circular ports at 45°, 90° and 135° to its longitudinal axis for non-invasive thermal and optical FFDP measurements. Inside the cryostat, there is an inner copper shield, painted with black Aeroglaze Z306 (0.95 emissivity and low out-gassing), which is kept at $T \sim 77$ K with liquid nitrogen. When the shield is cold, the vacuum is in the 10^{-6} mbar range. Two positioning systems at the top of the cryostat (one for planar movements and one for spherical rotations) hold the Laser Reflector Array (LRA) in front of the Solar Simulator (SS) and of the infrared (IR) camera, both located outside the SCF. An Earth infrared Simulator (ES) can be also made available inside the SCF. After SS/ES heating, LRAs are rotated about the vertical for laser tests from the 90° port. The CCR thermal relaxation time, τ_{CCR} , is measured with the IR camera through the 45° port, equipped with Ge window, during SS/ES heating and FFDP tests. FFDPs could be taken during ES/SS heating through the 45° port (replacing the Ge window with an optical one).

The SS beam enters through a quartz “AM0” window (37 cm diameter, 36 mm thickness), which, aside from Fresnel reflection losses, is transparent to

the solar radiation up to about 3 μm . This has been quantified with thermal modelling and validated auxiliary measurements and calibrations. The effect on CCRs of IR radiation absorbed for $\lambda > 3 \mu\text{m}$ is partly compensated by the IR reemitted by the warm AM0 window and 45°/90°/135° ports. Full compensation is to be achieved with IR emitters inside the SCF and/or thermal modelling.

The SS provides a 40 cm diameter beam with close spectral match to the AM0 standard. The spectrum is formed by a metal halide (HMI) arc lamp (UV-VIS; 6 kW), together with a quartz halogen, tungsten filament lamp (Red-IR; 12 kW). The uniformity of the SS intensity is $\pm 5\%$ over 35 cm diameter. The absolute scale of the intensity is maintained by exposing to the SS, a *solarimeter*, which is a standard thermopile (calibrated blackbody), accurate and stable over > 5 years to $\pm 2\%$.

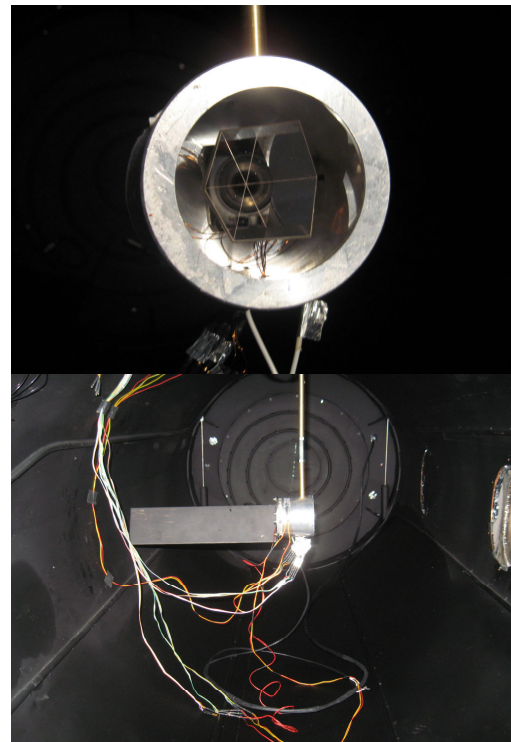


Fig. V: two pictures of the Pyrex CCR placed inside the SCF

Goddard Space Flight Center, sent in Frascati the hollow Pyrex CCR, for testing purpose. In Fig. V, there are two pictures of the CCR placed inside the thermo vacuum chamber of the SCF; the upper picture is a front view while the lower one shows the CCR tilted by 90° to be oriented in the direction of the laser window. The CCR is fixed inside a cylindrical aluminium housing: only one mirror is supported and the supporting frame is

screwed on the housing. Housing temperature has been kept, during measurements, at 300 K and it has been controlled through a thermo electric cooler; in the lower picture of Fig. V, you can see the wide cooling fin of the TEC standing out the back of the housing. There were 4 thermal probes: three glued on the back faces of the mirrors (one per each) and the fourth glued on the housing. We use class-A PT100 probes with 4-wire readout with standard accuracy and inter-changeability of 0.2 K.

The PT100s temperature scale is checked with a dry-block absolute temperature calibrator capable of ≤ 0.1 K accuracy and with custom-calibrated PT100 systems.

During measurements we applied a wider load cycle but, in the following, we are going to show just one completely representative portion of it. The mounted mirror (the blue curve) is thermally tied to the housing kept at fixed temperature, for this reason its temperature changes less than the others during the solar heat load. The other two mirrors, show a very close thermal behaviour.

Having experimental data available, we moved back to FEM simulations. The optical behaviour of the CCR was rather good during all the time so we expected both the peak to valley and the dihedral angle offset parameters to keep inside the boundaries $0.025 \mu\text{m}$ and $\pm 0.5^\circ$ respectively.

We implemented at first in ANSYS[®] a very simple thermal field: all the nodes belonging to one mirror were set at the same temperature measured by the probe.

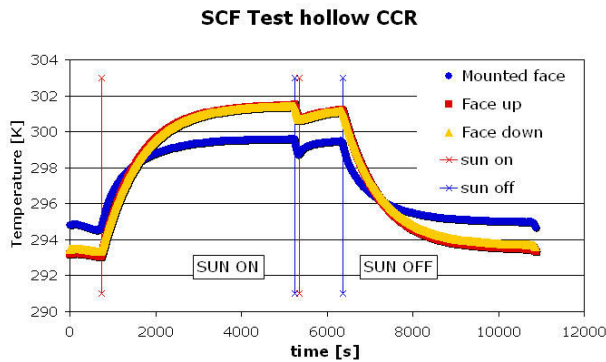


Fig. VI: Temperatures of the three mirrors

This approach turned to be too rough and we got values both for the peaks to valleys and for the dihedral angle offsets that were very far from the expected values. Since the manufacturer did not furnish reliable data for the glue we tried also to change its two key parameters i.e. the Young's module and the coefficient of thermal expansion over a very wide range but it has not been enough to cover the difference between simulated results and expected values.

In Fig. VII, we show the results of this parametric analysis just for the peak to valley of the mounted mirror and the dihedral angle offset between itself and one other of the remaining two mirrors. These computations were a little bit time consuming they really worth since clearly showed that the glue cannot be considered the only point to address.

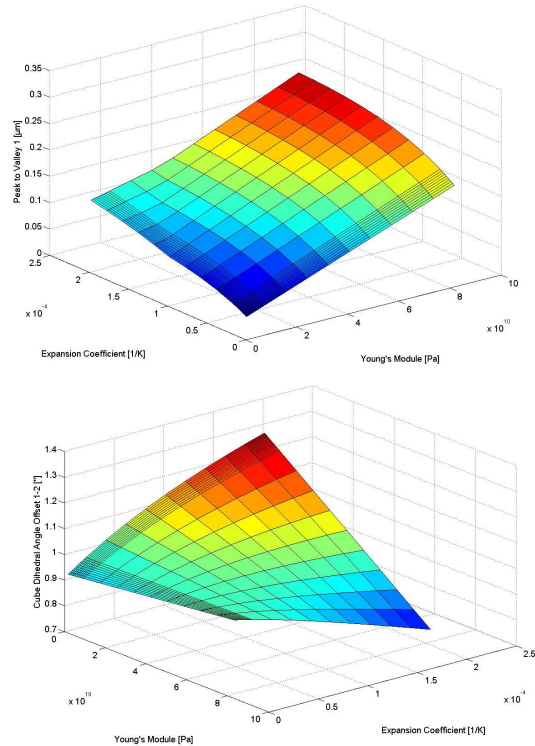


Fig. VII: Glue Young's module and CTE influence over the peak to valley and dihedral angle offset.

Thermal simulations with Thermal Desktop[®]

Pyrex has a rather low value for thermal conductivity and the supposed thermal field, with all the mirror nodes at the same temperature, is not suitable for the comprehension of the CCR behaviour. We then exported the ANSYS[®] finite element model inside Thermal Desktop[®], which is the software we use for thermal simulations. Inside this second simulation environment we set guess values both for the thermal conduction between the mounted mirror and the housing and for the heat conduction among the mirrors through the glue. We then exported back this realistic thermal field inside ANSYS[®] and computed again from the deformed model the peaks to valleys and the dihedral angle offset. We tested the complete gear of information transfer between the softwares and in Fig. VIII we show how the thermal field computed in Thermal Desktop[®] is properly transferred inside ANSYS[®].

Nevertheless, the solution from Thermal Desktop® is still not reliable since there are some parameters inside the model that have been set just to guess value. A fine tuning, trying to match temperature measurements and simulation results will be carried on in the next coming activities.

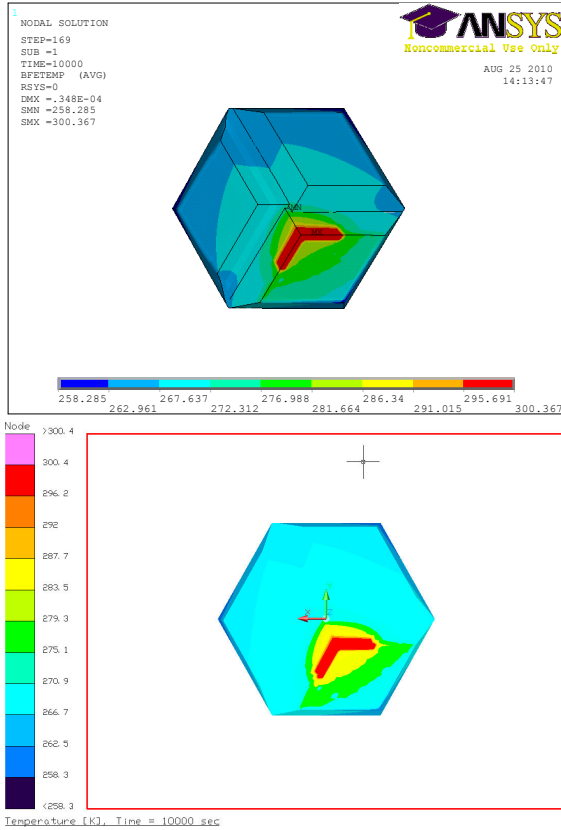


Fig. VIII: Thermal field computed with Thermal Desktop® is then transferred in ANSYS®

2nd order fitting surface

The same procedure we used to best fit the cloud of points with a plane, can be also used for a second order fitting surface. Let's consider the un-deformed mirror plane as the x-y plane of the coordinate system; the more suitable fitting surface has a saddle point in the origin and the points along the x and the y axes (which would represent the glued mirror edges) with no elevation. Such a surface has the following mathematical expression:

$$z = cxy$$

In Fig. IX we show a representation of such surface: the parameter “c” directly accounts for the elevation and we gave an exaggerated value just for explaining purpose.

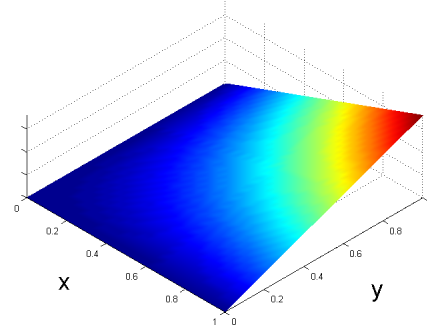


Fig. IX: Second order surface suitable for mirror deformation fitting

We believe that this approach, followed by proper optical simulations will lead to a better comprehension of the complex interaction between thermal loads, structural deformation and optical behaviour of hollow CCRs.

IV. CONCLUSIONS

Even though classical cube corner retroreflectors have always given, during very long years, their precious contribute to fundamental physics and space geodesy, the expanse involved by sending heavy objects in space, makes new generation hollow reflectors an attractive challenge.

The experimental apparatus set inside the Frascati National Laboratories of INFN, allows to check the optical performance of a laser reflector placed in a realistic space environment. The Frascati group has a strong experience both in simulation and testing of classical CCRs but, the work here showed about hollow cubes, comes to be original. They are reported in the paper the experimental temperature measurements on a Pyrex hollow CCR.

We considered three possible designs and carried on finite element structural simulations. One key aspect of the behaviour is the mechanical action that the adhesive transfers to the mirrors. For this reason we modelled the glue using two different approaches, complementary for precision and computation time. Nevertheless, the paper results clearly show that the glue cannot be considered the only point to address, while a finer characterization of the temperature distribution is necessary to correctly understand the structural deformation and therefore the optical performance.

An important enhancement in the comprehension of these optical devices could be to consider the deformed mirrors no longer fitted by flat planes but by second order surfaces with a saddle point in the intersection of the glued edges.

REFERENCES

- (1) *The International Laser Ranging Service*, Pearlman, M.R., Degnan, J.J., and Bosworth, J.M., *Advances in Space Research*, Vol. 30, No. 2, pp. 135-143, July 2002, DOI:10.1016/S0273-1177(02)00277-6. See also: <http://ilrs.gsfc.nasa.gov>.
- (2) *Creation of the new industry-standard Space Test of Laser Retro-reflector for the GNSS, Fundamental Physics and Space Geodesy: the SCF-Test*, S. Dell'Agnello et al, submitted to *Advances in Space Research*, Dec 2009.
- (3) *Technology challenges*, M. Pearlman, Int. Technical Laser Workshop on SLR tracking of GNSS Constellations, Metsovo(GR), Sept 2009.
- (4) *MoonLIGHT: Moon Laser Instrumentation for General relativity High-accuracy Tests*, G. Bellettini, D. G. Currie, S. Dell'Agnello, C. Cantone, G. O. Delle Monache, M. Garattini, N. Intaglietta, R. Vittori, INFN-LNF Reports LNF-06/28(IR), 2006, a project approved by NASA for the LSSO program, and LNF-07/02(IR), 2007, a lunar study funded by ASI. See also [http://www.lnf.infn.it/sis/preprint/pdf/getfile.php?filename=LNF-06-28\(IR\).pdf](http://www.lnf.infn.it/sis/preprint/pdf/getfile.php?filename=LNF-06-28(IR).pdf) and [http://www.lnf.infn.it/sis/preprint/pdf/getfile.php?filename=LNF-07-2\(IR\).pdf](http://www.lnf.infn.it/sis/preprint/pdf/getfile.php?filename=LNF-07-2(IR).pdf).
- (5) *Fundamental Physics and Absolute Positioning Metrology with the MAGIA Lunar Orbiter*, S. Dell'Agnello, R. Vittori, G. O. Delle Monache, D. G. Currie, G. Bellettini, A. Boni, C. Cantone, M. Garattini, N. Intaglietta, R. March, M. Martini, M. Maiello, C. Lops, C. Prosperi, R. Tauraso, submitted to *Experimental Astronomy*.
- (6) *Next Generation Lunar Laser Ranging and its GNSS Applications*, S. Dell'Agnello, A. Boni, C. Cantone et al, 2010 IEEE Aerospace conference.
- (7) *Design and Construction of a Laser-Ranged Test Mass for the Deep Space Gravity Probe Mission and Test of a Hollow Retroreflector for the GPS-3*, S. Dell'Agnello et al, <http://www.lnf.infn.it/sis/preprint/detail.php?id=5139>
- (8) *Proposed Single Open Reflector for the GALILEO Mission*, R. Neubert, et al., International Technical Laser Workshop on SLR tracking of GNSS Constellations, Metsovo(GR), Sept 2009.
- (9) *Uncoated Cubes for GNSS satellites*, D. Arnold, Int. Technical Laser Workshop on SLR tracking of GNSS Constellations, Metsovo(GR), Sept 2009.